JCTC Journal of Chemical Theory and Computation

Article

pubs.acs.org/JCTC

Optical Properties of Diarylethenes with TD-DFT: 0−0 Energies, Fluorescence, Stokes Shifts, and Vibronic Shapes

Agisilaos Chantzis,[†] Javier Cerezo,[‡] Aurélie Perrier,[§] Fabrizio Santoro,*[,∥] and Denis Jacquemin*[,†,⊥]

[†]Laboratoire CEISAM - UMR CNR 6230, Université de Nantes, 2 Rue de la Houssiniére, BP 92208, 44322 Nantes Cedex 3, France

[‡]Departamento de Química Física, Universidad de Murcia, 30110 Murcia, Spain

[§]ITODYS, UMR 7086, Université Paris Diderot, Sorbonne Paris Cité, 15 Rue Jean Antoine de Baif, 75205 Paris Cedex 13, France

[∥]CNR−Consiglio Nazionale delle Ricerche, Istituto di Chimica dei Composti OrganoMetallici (ICCOM-CNR), UOS di Pisa, Area della Ricerca, via G. Moruzzi 1, I-56124 Pisa, Italy

[⊥]Institut Universitaire de France, 103, bd Saint-Michel, F-75005 Paris Cedex 05, France

Supporting Information

ABSTRACT: This contribution is an investigation of both the structures and optical properties of a set of 14 diverse, recently synthesized diarylethenes using Time-Dependent Density Functional Theory (TD-DFT) at the ωB97X-D/6-31G(d) level of theory. The linear response (LR) and state-specific (SS) versions of the Polarizable Continuum Model (PCM) have been adopted to account for the bulk solvation effects and their relative performances were critically accessed. It is shown, for the first time in the case of nontrivial diarylethenes, that TD-DFT provides good agreement between the experimental absorption-fluorescence crossing points (AFCPs) and their theoretical counterparts when a robust model accounting for both geometrical relaxation and vibrational corrections is used instead of the vertical approximation. On the other hand, the theoretical estimates for the Stokes shifts based on the vertical transition energies were found to be in disagreement with respect to experiment, prompting us to simulate the absorption/emission vibronic band shapes. It is proved that difficulties associated with the breakdown of the harmonic approximation in Cartesian coordinates exist for the investigated system, and we show how they can be at least partially overcome by means of a vertical approach including Duschinsky effects. Our results provide a valuable basis to rationalize the experimental vibronic structure of both emission and absorption bands and are expected to be a significant asset to the understanding of the optical properties of diarylethene derivatives.

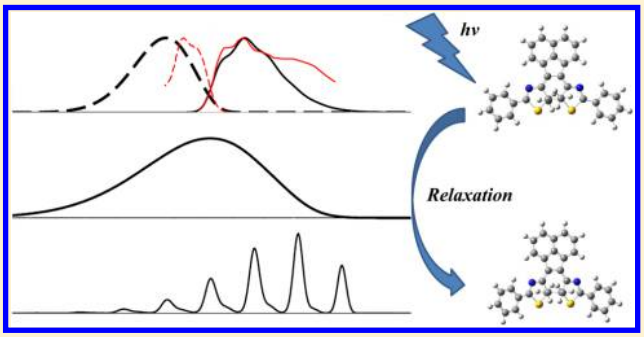

1. INTRODUCTION

Molecular systems exhibiting photochromism, that is, a photoinduced reversible transformation between two forms having different properties (absorption spectrum, refractive index, dielectric constant, fluorescence spectrum, etc.), have attracted a constantly increasing interest due to their potential applications in technology and materials science.[1−5] Nowadays, the photochromic molecules that are most intensively investigated are members of the azobenzene, diarylethene, dihydroazulene, dihydroperene, fulgide, fulgimide, napthopyran, spiropyran, spiroxazine, and vinylheptafulvene families. Among them, the most interesting thermally stable compounds for both fundamental research as well as for technological applications belong to the diarylethene series, as can be easily witnessed by a large number of reviews and monographs.[6−16] Diarylethenes have been introduced by the groups of Irie[17−19] and Lehn[20] and were shown to undergo a reversible photoinduced isomerization between an open colorless form having a hexatriene structure and a closed colored form presenting a cyclohexadiene core, the transformation qualitatively following the Woodward−Hoffmann rules.[21] Both isomers are thermally stable under standard conditions; the thermal isomerization being prohibited by large activation barriers. Irradiation with UV light facilitates the ring closure reaction (cyclization) while the ring-opening (photoreversion) is induced by irradiation with visible light. Numerous investigations have indicated that diarylethenes constitute one of the most important families of single-molecule photochromes that can yield practical applications due to their very large fatigue resistance, thermal irreversibility, distinctively different properties between the two isomers, short response times, and high quantum yields. Lately, exciting applications of diarylethene photochromism in biology have appeared, making possible living cell imaging, labeling and imaging of biomolecules, as well as photocontrol of biological systems.[11,22−25] In data storage applications, thermal stability and the difference in properties of the two isomers can be used

Received: April 29, 2014
Published: May 21, 2014

 © 2014 American Chemical Society dx.doi.org/10.1021/ct500371u | J. Chem. Theory Comput. 2014, 10, 3944−3957

Scheme 1. Representation of the Investigated Diarylethenes

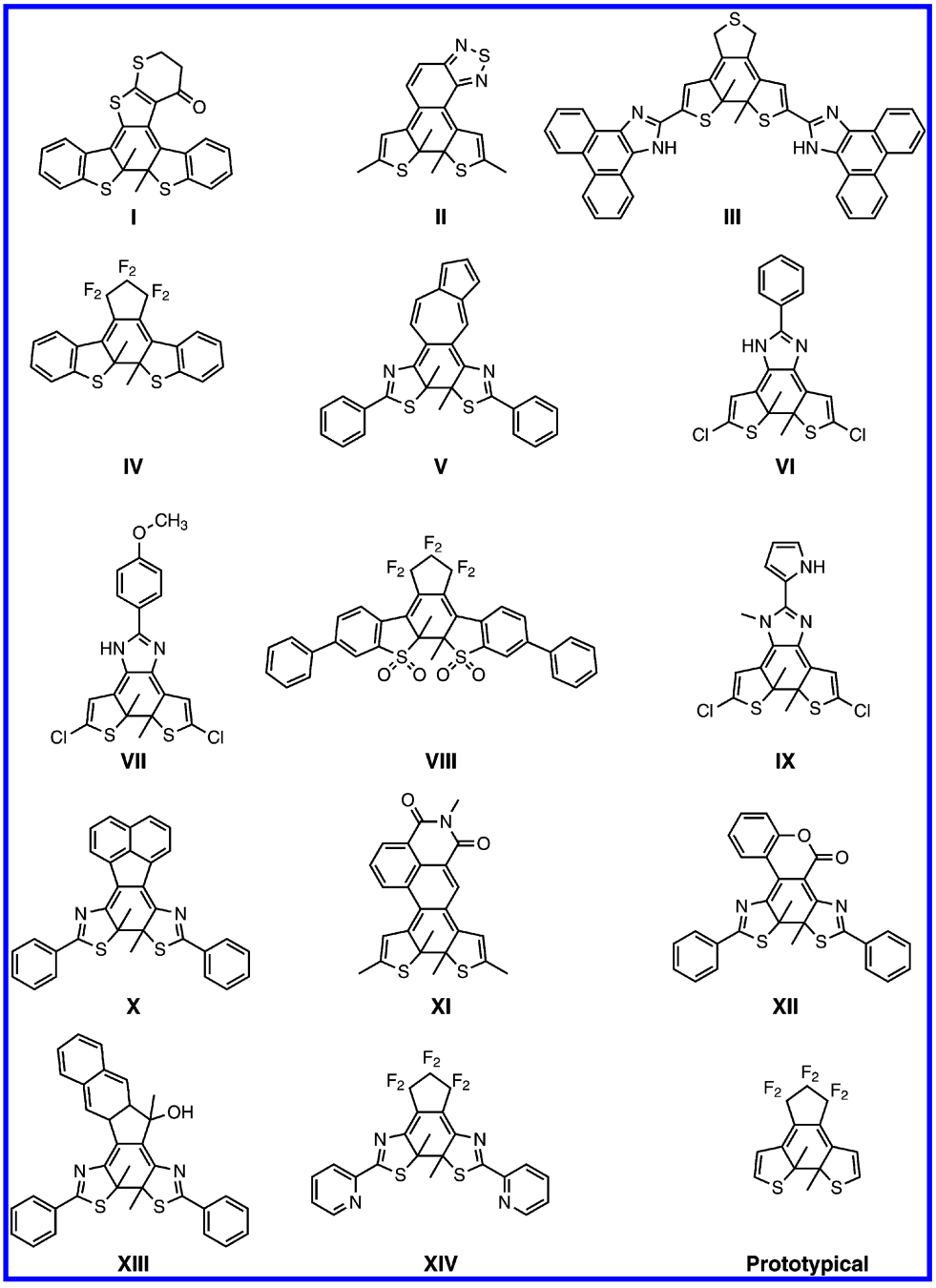

to store information as an alternative to traditional devices.[2,3,16,26,27]

Among the properties that are being utilized for both data recording and imaging is fluorescence. In the case of single-molecule fluorescence photoswitching, fluorophores are attached to a diarylethene photochrome and quenching of emission following the photochromic reaction is observed. Indeed, in most cases there is a severe quenching of fluorescence intensity upon photocyclization, while fluoresence can be restored by photoreversion.[28] Nevertheless, there are several cases that have been reviewed recently for which the reverse behavior is observed or for which both isomers display fluorescence.[11] The most well-grounded mechanism proposed to explain fluorescence quenching is the intramolecular transfer of charge or energy from the fluorophore to the diarylethene moiety after photoexcitation of the former to its singlet state. Closely related to fluorescence modulation is fluorescence nondestructive readout of data stored in diarylethene based memories. In these devices, it is important that fluorescence detection for data readout occurs at wavelengths at which neither isomer of the diarylethene unit absorbs and consequently reacts. This in turn implies that the absorption spectra of both closed and open isomers should not overlap at all with the emission spectra of the fluorophore, a requirement that is not easy to meet for most diarylethenes. In order to facilitate the independent modulation of photochromic reactions and fluorescence detection, several methodologies have been devised. One recently proposed by Fukaminato et al. stands out as quite promising, at least at the single-molecule level.[29]

dx.doi.org/10.1021/ct500371u | J. Chem. Theory Comput. 2014, 10, 3944−3957

Besides the knowledge gained through extensive experimental studies, modern electronic structure theories are able to contribute to the understanding of reactivity and properties of both dyes and photochromes. The investigations span diverse fields including the elucidation of the reactivity of diarylethenes considering both ground (GS) and excited states (ES),[30,31,31−41] the rational design of coupled photochromes[16,42−47] (dyads, triads, etc.), the simulation of molecular wires,[48] and the understanding of the properties of diarylethenes either attached to gold clusters[49] or bridging two carbon nanotubes.[50] There exist also numerous studies reporting on the optical absorption spectrum of a wide range of diarylethenes, mainly at the Time-Dependent Density Functional Theory (TD-DFT) level which has become the *de facto* standard in the field of optical spectra of large molecules. Most TD-DFT spectroscopic studies adopt the vertical approximation due to the high computational cost of other more accurate and complete approaches.[51−59] For instance, the determination of 0−0 energies, which have been repeatedly shown to be more appropriate for theory/experiment comparisons[60−62] requires the calculation of the ES TD-DFT Hessian. Therefore, no systematic study of the performance of TD-DFT for the computation of 0−0 energies has been performed in the past for this class of photochromes, and the present study aims predominantly to fill this gap. In addition, only a very few TD-DFT investigations have tackled the emission wavelengths of diarylethenes.[40] Moreover, it is also of immediate interest to investigate the predictive capability of the vertical transition approximation in providing reliable predictions for the Stokes shifts so as to guide experiment studies aiming at fluorescence modulation.

In the present contribution, we report an extensive study on the 0−0 energies and Stokes shifts of a panel of 14 structurally diverse diarylethene molecules with TD-DFT. The set of investigated molecules along with the solvents used in experiments can be found in Scheme 1 and in Table 1,

Table 1. List of Solvents Used along with the Respective Experimental References

molecule	solvent	ref.	molecule	solvent	ref.
I	ethylethanoate	23	**VIII**	1,4-dioxane	63
II	cyclohexane	64	**IX**	acetonitrile	65
III	dimethyl sulfoxide	66	**X**	*n*-hexane	67
IV	ethylethanoate	68	**XI**	cyclohexane	69
V	*n*-hexane	70	**XII**	*n*-hexane	71
VI	acetonitrile	72	**XIII**	ethylethanoate	73
VII	acetonitrile	72	**XIV**	acetonitrile	74

respectively (note that, for **XI** the *n*-butyl group attached on the N atom has been changed to a methyl group for reasons of computational efficiency). In the present work, we have focused solely on the closed isomers of the systems with a 2-fold aim: (i) the assessment of TD-DFT in reproducing the experimentally observed 0−0 energies and Stokes shifts, an endeavor that has not been undertaken in the past for diarylethenes, and (ii) an investigation on the possible existence of a relationship between chemical structure and the optical properties. Moreover, different models that are routinely used to model bulk solvent effects were applied in order to indicate the one best matching the experimental findings for this specific class of switches. Additionally, in order to investigate to what extent predictions of maxima and Stokes shifts based on vertical transitions are modified by accounting for vibronic effects, the study has been completed by simulating the vibronic shape of the absorption and emission bands for some compounds, including Duschinsky effects according to both adiabatic and vertical models.

2. COMPUTATIONAL DETAILS

Full details of our computational methodology along with a definition of all relevant quantities have been reported previously,[62] and thus, only an outline is given here. All computations reported herein were performed using TD-DFT/DFT at the ωB97X-D/6-31G(d)[75] level of theory using the Gaussian09.C01 program.[76] Benchmark calculations have also been performed using the ωB97 and ωB97X functionals[77] as well as the 6-311+G(2d,p) atomic basis set. Full geometry optimizations for both the GS (ground state singlet, S_0) and ES (first and second excited state singlets, S_1 and S_2) followed by the calculation of harmonic frequencies at the respective minima were carried out in order to compute the 0−0 energies while the Stokes shifts were computed by subtracting vertical absorption and emission energies and converting to the wavelength or wavenumber scale. The GS frequencies were computed analytically while the ES ones numerically due to the lack of analytic second derivatives for TD-DFT in Gaussian 09. All geometry optimizations have been carried out with the Berny-GEDIIS[78] algorithm with the tight convergence criteria (10^{-5} au for the RMS force) utilizing analytic first derivatives for both states of interest, while the SCF convergence criterium was set to at least 10^{-9} au. In all cases, a standard pruned Euler−Maclaurin−Lebedev integration grid has been chosen, which consists of 75 radial and 302 angular points per atom. For the calculation of the anharmonic frequencies, the second-order perturbative approach[79] as implemented in Gaussian 09 was used, employing the default step size of 0.025 Å for the numerical differentiations. For modeling bulk solvation effects the Polarizable Continuum Model (PCM) model was used in its linear response formalism (LR)[80] for geometry optimizations and frequency calculations whereas both the LR and state-specific (SS)[81,82] formalisms were applied to compute transition energies. The G09 defaults for the PCM cavity definitions have been retained in all calculations. Vibrationally resolved electronic spectra were simulated at 298 K within the harmonic approximation. Beyond the popular Adiabatic Hessian (AH) model, we adopt also the vertical Hessian (VH) one,[83] since we will show that AH Cartesian coordinates fails to properly linearly relate GS and ES modes for the systems under investigation, eventually leading to an excessive broadening of the spectra. In addition to the frequency calculations indicated above, for the simulation the absorption/emission spectra, the VH model requires the computation of GS/ES Hessian at the Franck−Condon region (i.e., ES/GS minima). In fact, while the initial state PES of the optical transition is always quadratically expanded around its minimum, the final state PES is expanded either around its minimum (AH), or around the initial state minimum, that is, the Franck−Condon region (VH). Finite-temperature spectra were computed by means of the time-dependent (TD) formulation implemented in a development version of the program *FCclasses*,[84,85] as the Fourier transform of the time correlation function evaluated every 0.12 fs up to 500 fs, and adding a Gaussian broadening function with a half-width at half-maximum (HWHM) in the frequency domain of 0.03 eV. To support our analysis, Time Independent (TI) spectra at 0 K,

which allow to analyze each individual transition in terms of the normal modes, were computed with the prescreening method implemented in *FCclasses*.[86] In order to allow a trustful comparison of our theoretical predictions with the available experimental spectra, the latter were modified to map the original data in wavelength units into the wavenumber domain by applying the adequate factors (ν^{-2} for emission) and then further modified to obtain the lineshapes (factors ν^{-1} for absorption and ν^{-3} for emission).[87]

3. SUBSTITUTION EFFECTS

3.1. Geometrical Properties in GS and ES. The set of closed diarylethenes for which geometry optimizations were performed in both the GS and ES is shown in Scheme 1. The substitution patterns can be seen to fall in one of the three following categories: (i) substitution on the 5 and 5′ positions of the thiophene rings; (ii) substitution on the perfluoro cyclopentane bridge; and (iii) alterations on the chemical nature of the perfluoro cyclopentane bridge. The two latter categories will be treated in the following as a single set, since they effectively comprise different substitutions around the central cyclohexadiene core. In order to quantify the geometrical changes induced by the different substituents in the GS or the geometrical relaxation in the ES, the two dihedral angles ϕ_1 and ϕ_2 along with the r_{CC} distance defined in Figure 1 were used.

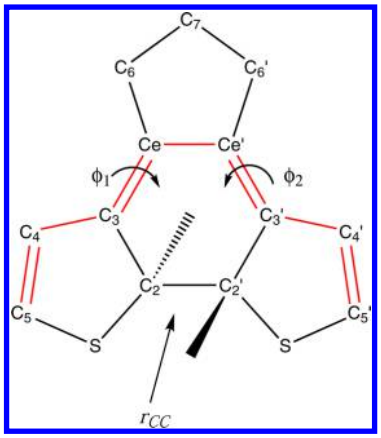

Figure 1. Atom numbering along with definitions of important geometrical parameters used in the text. The distance between carbon atoms 2 and 2′ is r_{CC} while the dihedral angles ϕ_1 and ϕ_2 are defined as the $e'-e-3-2$ and $e-e'-3'-2'$ angles, respectively. The BLA path is defined by the red-colored bonds.

Since a one-to-one correspondence between the dihedral angles of different molecules cannot be established, we have used the following quantities for each molecule k:

$$\Delta\phi(\mathrm{GS}) = \left|\sum_{i=1}^{2} \phi_i^k(\mathrm{GS}) - \sum_{i=1}^{2} \phi_i^{\mathrm{proto}}(\mathrm{GS})\right| \quad (1)$$

$$\Delta\phi(\mathrm{ES}) = \left|\sum_{i=1}^{2} \phi_i^k(\mathrm{ES}) - \sum_{i=1}^{2} \phi_i^k(\mathrm{GS})\right| \quad (2)$$

In the expressions given above, GS and ES refer to the optimal structures for the ground and first excited state respectively, ϕ_i^k is the dihedral angle i of molecule k while ϕ_i^{proto} stands as the dihedral angle i of the prototypical system (see Scheme 1). Additionally, the so-called bond length alternation (BLA) parameter that is useful when discussing the extension of π-electron (de)localization along a structure with alternating single and double bonds, has been determined. In the case of diarylethenes in their closed form, BLA can be defined, for either the GS or the ES, based on the path shown in Figure 1:

$$\mathrm{BLA} = \sum r_{\mathrm{single}} - \sum r_{\mathrm{double}} = r_{34} + r_{ee'} + r_{3'4'} - r_{45} - r_{3e} - r_{3'e'} - r_{4'5'} \quad (3)$$

where the sums run all over single and double bonds in the π-conjugated path. Since for the molecules considered here, there exist three single and four double bonds, the BLA values will be negative. As the degree of π-electron delocalization increases, the length of the single (double) bonds along the path will decrease (increase), and consequently, the BLA value will become more negative, while in more localized π-electron systems, the BLA will take larger values tending to zero. A scaled BLA parameter that is simply defined as[89]

$$\mathrm{BLA}_{\mathrm{scaled}} = (\mathrm{BLA} + 1) \times 10 \quad (4)$$

has also been used here. All the relevant quantities along with the reactive carbon bond distance, r_{CC} (see Figure 1), for the GS and the ES can be found in Tables 2 and 3, respectively. Since not a unique solvent was used for the whole set of molecules, it is not possible to strictly separate the geometrical effects caused by substitution from those related to the solvent. Nonetheless, it can be seen from Supporting Information Table S-I for **IV** and **XIV** that the substitution effects are clearly the dominating factors for geometrical changes both in the GS and the ES.

Focusing on the GS geometrical properties one can readily notice that the r_{CC} distance is practically unaltered for the whole set with respect to the one found in the reference diarylethene, the differences ranging from 0.04 to 0.52%. This in turn indicates that substantial modifications of the structure can occur without the risk of breaking the ring and this finding is consistent with the diversity of stable diarylethene derivatives. Indeed, it has been shown that there is a relationship between r_{CC} and the thermal stability of the closed form.[13,55] On the other hand, the cyclohexadiene core undergoes major geometrical changes as can be readily seen from the $\mathrm{BLA}_{\mathrm{scaled}}$ and $\Delta\phi$ values of Table 2. For $\Delta\phi$, the largest changes (ca. 92% of the reference value) with respect to the unsubstituted system can be found for molecules **I**, **XI**, and **XII**. It can be argued that the largest geometrical distortions seem to be caused, for the majority of cases, by tuning both the perfluoro bridge and the thiophene rings. Leaving the bridge intact and modifying the thiophenes (see **IV**, **VIII**, and **XIV**) only yields minor geometrical rearrangements of the core compared to the prototype compound. These trends agree with chemical intuition. The relative $\mathrm{BLA}_{\mathrm{scaled}}$ varies widely (2.5−202%) for the systems of the set: all show more extended delocalization than the reference system except for **X** and **XIII**, with molecules **I**, **IV**, and **VIII** being the most effectively conjugated structures. One can deduce that there is no simple relationship between the degree of geometrical distortions ($\Delta\phi$) and the extent of π-conjugation (BLA). To explain this outcome, one has to recall how the BLA was defined. It can be readily seen there that the BLA path also involves the thiophene rings whereas $\Delta\phi$ only accounts for changes induced on the cyclohexadiene core.

Passing to the excited state geometries, it is clear from Table 3 that all molecules undergo major geometrical changes compared to the ground state structures. First, the r_{CC} relative

dx.doi.org/10.1021/ct500371u | J. Chem. Theory Comput. 2014, 10, 3944−3957

Table 2. Geometrical Parameters of the Studied Molecules at Their Optimized GS Geometries

system	symmetry	BLA (Å)	BLA_{scaled} (Å)	ϕ_1(deg)	ϕ_2 (deg)	r_{CC} (Å)	$\Delta\phi$ (deg)
I	C_1	−1.135	−1.35	−1.9	−24.1	1.538	12.5
II	C_1	−1.060	−0.60	−6.2	−6.8	1.534	0.6
III	C_1	−1.070	−0.70	−6.6	−6.7	1.540	0.2
IV	C_1	−1.123	−1.23	−2.2	−11.8	1.542	0.4
V	C_1	−1.063	−0.63	−5.1	−5.6	1.533	2.9
VI	C_1	−1.057	−0.57	−8.9	−8.3	1.544	3.6
VII	C_1	−1.054	−0.54	−8.0	−8.1	1.545	2.5
VIII	C_1	−1.097	−0.97	−2.2	−11.7	1.549	0.3
IX	C_1	−1.055	−0.55	−8.7	−6.7	1.543	1.8
X	C_2	−1.028	−0.28	−7.4	−7.4	1.543	1.1
XI	C_1	−1.061	−0.61	−5.2	1.9	1.537	10.3
XII	C_1	−1.062	−0.62	−2.5	−3.1	1.536	8.1
XIII	C_1	−1.044	−0.44	−8.7	−8.8	1.542	3.9
XIV	C_1	−1.059	−0.59	−6.8	−6.4	1.543	0.4
prototypical	C_1	*−1.045*	*−0.45*	*−6.3*	*−7.3*	*1.541*	*0.0*

Table 3. Geometrical Parameters of the Studied Molecules at Their Optimized ES Geometries

system	symmetry	BLA (Å)	BLA_{scaled} (Å)	ϕ_1 (deg)	ϕ_2 (deg)	r_{CC} (Å)	$\Delta\phi$ (deg)
I	C_1	−1.404	−4.04	−12.4	−29.0	1.605	15.3
II	C_1	−1.335	−3.35	−15.9	−14.7	1.597	17.6
III	C_1	−1.477	−4.77	−13.7	−13.7	1.567	14.0
IV	C_1	−1.432	−4.32	−8.5	−16.4	1.599	10.9
V	C_1	−1.252	−2.52	−9.4	−10.0	1.558	8.7
VI	C_1	−1.342	−3.42	−14.9	−14.6	1.598	12.3
VII	C_1	−1.343	−3.43	−15.0	−14.6	1.598	13.5
VIII	C_1	−1.427	−4.27	−7.5	−18.1	1.574	11.8
IX	C_1	−1.343	−3.43	−13.6	−14.2	1.593	12.4
X	C_2	−1.346	−3.46	−12.9	−12.9	1.584	11.1
XI	C_1	−1.293	−2.93	0.1	−10.6	1.567	7.1
XII	C_1	−1.397	−3.97	−16.8	−16.9	1.590	28.2
XIII	C_1	−1.391	−3.91	−16.1	−13.0	1.583	11.7
XIV	C_1	−1.415	−4.15	−13.3	−13.0	1.589	13.1
prototypical	C_1	*−1.328*	*−3.28*	*−13.5*	*−14.7*	*1.629*	*14.6*

values are much larger for the ES. Indeed, they increase by 1.6 to 12% upon excitation, indicating significant elongation of the bond following the initial photoexcitation. Interestingly, the same trend is observed also for $\Delta\phi$, for which very large changes are observed, the relative variations ranging from 59 to 509%. On average, the absolute values increase by ca. 13°—a large value for such constrained systems. Moreover, there is significant redistribution of the π-electrons along the path of Figure 1, as witnessed by the large changes between the BLA values between the GS and ES minima. Evidently, even this totally static picture indicates the possibility of cycloreversion by cleavage of the r_{CC} bond and redistribution of the π-electrons of the system, a trend that seems general and independent of the structure of each diarylethene. This latter observation might be used, along with the topology of the HOMO and LUMO orbitals in the Franck−Condon (FC) region, as an additional criterium for the presence (or lack thereof) of photochromism in substituted diarylethenes. Importantly, the significant differences found for all systems between the GS and ES geometries warn for the potential inadequacy of the vertical approximation in computing optical data, an issue that will be addressed in the following.

4. OPTICAL SPECTRA

In this section, theoretical estimates for the vertical transition energies, 0−0 energies and Stokes shifts are reported using a variety of continuum solvation models at the ωB97X-D/6-31G(d) level of theory and comparisons with available experimental data are made. Benchmark studies performed in order to safeguard the reliability of our results can be found in the Supporting Information. It has to be noted that although experimental estimates for λ_{max} were available for all studied molecules, experimental fluorescence spectra could be obtained for only a few of them. The reason is that most of the closed-ring isomers does not show any fluorescence or the fluorescence is clearly due to states higher than the S_1, violating thus Kasha's rule. For the remaining systems, namely **I**, **VIII**, and **X**, it is not clear from experiment which state is involved in the emission and this prompted us to investigate this issue thoroughly. To this end, we have performed calculations of the 0−0 energies and Stokes shifts based on both the S_1 and S_2 (see below).

4.1. Vertical Transition Energies. In this section, theoretical estimates of λ_{max} for both absorption and emission are reported and compared to the experimental data. We are aware, though, of the shortcomings in using the λ_{max} as a reference value to benchmark theoretical vertical energies (E_v), and that other descriptors, namely the first moment of the

Table 4. Theoretical Vertical Transition Energies Using Different Solvation Models along with Experimental Maxima of Absorption and Emission[a]

system	E^{abs}(LR,eq)	E^{abs}(LR,neq)	E^{abs}(SS,eq)	E^{abs}(SS,neq)	$\lambda^{abs}_{max,\ Exp.}$	E^{fluo}(LR,eq)	E^{fluo}(SS,eq)	E^{fluo}(SS,neq)	$\lambda^{fluo}_{max,\ Exp.}$
I	18 656	19 156	19 607	19 712	19 231	10 437	11 461	11 429	17241 (17082)
II	19 882	19 882	20 269	20 269	20 576	12 042	12 494	12 494	
III	19 075	19 753	20 083	20 156	17 123	9856	11 518	11 493	
IV	22 124	22 519	22 495	22 737	18 868	13 961	14 712	14 663	
V	16 591	16 591	16 768	16 768	14 286	8920	9138	9138	
VI	18 527	19 470	19 761	19 954	19 231	10 848	12 260	12 195	
VII	18 889	19 817	20 156	20 317	18 762	11 042	12 485	12 437	
VIII	24 923	24 971	25 415	25 423	22 573	17 768	18 478	18 478	19474 (18363)
IX	18 736	19 672	20 059	20 172	17 483	11 308	12 800	12 768	
X	20 970	20 962	21 261	21 261	18 083	13 857	14 308	14 308	14706 (13909)
XI	18 204	18 204	18 260	18 252	15 949	12 929	13 227	13 227	
XII	20 640	20 640	20 857	20 857	17 744	11 300	11 631	11 631	
XIII	20 898	21 374	21 753	21 850	19 011	12 703	13 832	13 808	
XIV	20 616	21 277	21 664	21 858	18 349	11 872	13 389	13 332	
MSE	1533	1930	2224	2308		−3120	−2391	−2402	
MAE	1815	2040	2268	2352		3120	2391	2402	

[a]All quantities are given in cm^{-1}. Maxima of the experimental lineshapes are reported in parentheses when they differ from the maxima of the spectra. At the bottom of the table, mean signed and mean absolute errors (MSE and MAE, respectively) are given considering the maxima of the spectra as references.

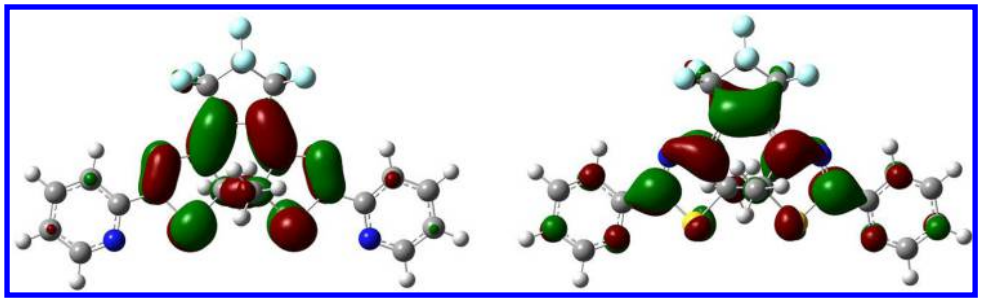

Figure 2. Occupied (left) and virtual (right) NTO corresponding to the $S_0 \rightarrow S_1$ transition of **XIV** in its GS geometry. The selected contour threshold is 0.03 au.

spectra (M_1), should be preferably used.[87] However, the accurate experimental computation of M_1 requires complete and nonoverlapping electronic bands, which is not normally available from experiments, and for the case of diarylethenes, we have observed that the position of M_1 (when it was possible to compute it) lies very close to λ_{max}. This finding supports the fair comparison of E_v and λ_{max}. As the impact of the solvent on the optical signatures of chromophores is well-known to be important, we have employed both the LR and SS continuum solvation models in their equilibrium and non equilibrium limits and the results are collected in Table 4.

Focusing first on the absorption data, it appears that it makes little difference whether one utilizes an equilibrium or nonequilibrium solvation limit for a specific PCM model (LR and SS). More specifically, the absolute relative errors with respect to the experimental λ_{max} for absorption range from 2.9% to 18.4% (0.3% to 18.4%) on the energy scale, for the case of LR equilibrium (nonequilibrium), whereas the respective SS errors are 1.1−18.2% (2.1%-18.8%). It is evident from these error panels that, for this class of compounds, the presumably more accurate but computationally expensive SS model does not lead to a systematic significant improvement of the theory-experiment match, at least for the case of absorption data listed in Table 4.

For the cases where a nonpolar solvent is used the near equivalence of equilibrium and nonequilibrium response is of course expected. For the cases where a solvent with a high dielectric constant is used, it is to be anticipated that different excitation energies will be calculated, depending on the applied PCM limit (equilibrium or nonequilibrium). For the present investigation, the insensitivity of the results toward the treatment of dynamical response of the solvent can be explained, for cases where a polar solvent is used, by realizing that irrespectively of the particular chemical structure of each diarylethene, the $S_0 \rightarrow S_1$ transition leads to electronic redistribution localized on the cyclohexadiene core and does not strongly influence the polarity of the molecule. This spatially confined charge rearrangement can be clearly seen for the case of system **XIV** in Figure 2 for which the Natural Transition Orbitals (NTOs)[89] for the $S_0 \rightarrow S_1$ transition are drawn. Besides this qualitative justification, numerical results for systems **III** and **XIV**, for which very polar solvents are used, also explain this insensitivity. Indeed, the electric dipole moment (disregarding the influence of the solvent) changes by only 9.1 and 1.9% with respect to their GS values of 4.44 and 4.38 D when going to the excited state for **III** and **XIV**, respectively. Moving now to an analysis of the relative performances of the different solvation models themselves, it has to be mentioned that the theoretical vertical excitation energies are more sensitive to the model used to treat the solvent (LR or SS) than to the inclusion or not of the dynamic response of the solvent (eq or neq). Notably, the insensitivity

dx.doi.org/10.1021/ct500371u | J. Chem. Theory Comput. 2014, 10, 3944−3957

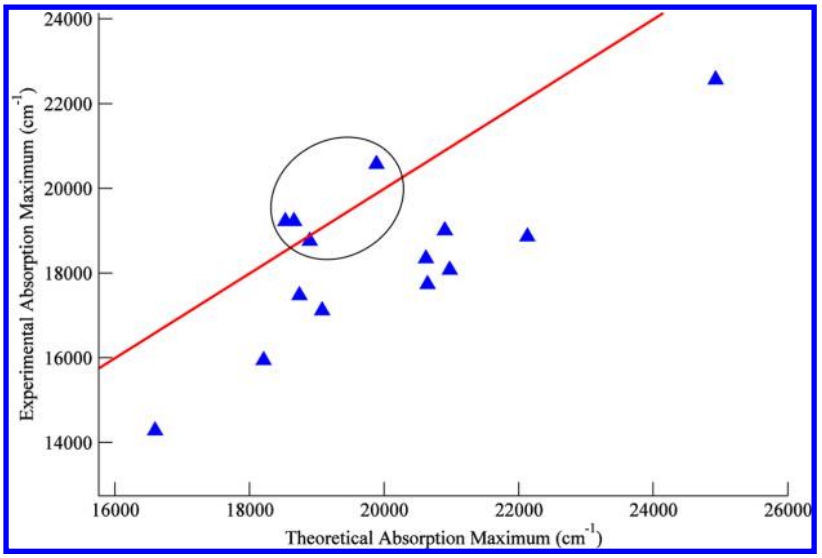

Figure 3. Correlation diagram between experimental and theoretical absorption maxima of systems **I**−**XIV** using the (LR,eq) solvation model. All quantities are given in cm^{-1}. The determination coefficient R^2, when systems contained in the oval line are excluded is 0.938.

to the dynamic response results in low reorganization energies which, according to Marcus theory, should induce a small solvent inhomogeneous broadening,[90] in agreement with the observed width of the experimental bands. The more refined SS model leads to an increase of the theoretical estimates by 0.3−7.1% and 0.3−2.9% with respect to the LR ones for the equilibrium and nonequilibrium limits, respectively, that is, rather limited variations.

Besides the comparisons between theory and experiment in terms of relative errors, it is also very useful to calculate the determination coefficient R^2 between experimental values and theoretical estimates of absorption λ_{max} so as to pinpoint emerging trends. For the case of (LR,eq), this is done in Figure 3 where a tendency of theory to overestimate the corresponding experimental transition energies is revealed, a nonsurprising outcome for ωB97X-D functional.[91] A close inspection of Figure 3 reveals that systems **I**, **II**, **VI**, and **VII** (triangles contained in the oval line) have strikingly good agreement with the experiment and do not cluster with the rest of the compounds. This dual behavior also reflects on the R^2 value of 0.566 which indicates a low correlation between the data sets. The same is found for the rest of the solvation models (see Figures S-1−S-3 in Supporting Information). This has prompted us to investigate more thoroughly the aforementioned molecules. For systems **I** and **II**, the spectra used to extract the experimental λ_{max} were particularly broad without a well-defined maximum. In fact, the 18900−20400 and 16600−22200 cm^{-1} spectral regions of the lowest energy absorption band of **I** and **II**, respectively, are of nearly constant intensity.[23,64] Therefore, establishing definitive conclusions on the basis of such ill-defined λ_{max} is not possible, at least when only vertical transition energies are computed. For the two remaining molecules, namely **VI** and **VII**, the experimental absorption maxima are well-defined and so experimental uncertainties cannot be the reason for the low correlation. In order to find the source of disagreement, we have calculated the vertical excitation energies, using the (LR,eq) solvation model, for different conformers of **VI** and **VII** by rotating the phenyl and methoxy groups, respectively. For both systems relative energies of the rotamers were found to lie in the 0.04−4.07 kcal mol^{-1} range, indicating nearly free rotation of these mobile groups not present in other compounds. Such rotation induces variations of the vertical absorption energies in the 20−461 cm^{-1} range. These small variations can only partly account for the theory-experiment discrepancies. Nevertheless, it has to be noted at this point that molecule **IX** although structurally similar to **VI** and **VII** cannot show free rotation of the pyrrole substituent due to the steric hindrance caused by the nearby methyl group. We have also examined the NTOs of these three systems and found no significant differences (see Supporting Information). Though the dynamic fluctuations cannot fully explain the difficulty to model **VI** and **VII**, it is striking that a very good correlation between the data is revealed when these two points are removed from the correlation (in addition to **I** and **II**), as witnessed by the R^2 for (LR,eq) solvation which is equal to 0.938. The R^2 for the other solvation models is even slightly larger, the value of 0.975 for (SS,eq) being the largest (see Figures S-2−S-4 in Supporting Information).

Moving to theory-experiment comparisons for the emission wavelength, the available data suggest that the vertical approximation is more case dependent than absorption results. From the contents of Table 4, it becomes obvious that irrespectively of the level of sophistication used for the treatment of solvation, the errors exceed 30% of the experimental value in the case of molecule **I** while for **VIII** and **X** the errors are significantly lower. This is most probably not due to an erratic performance of our theoretical model as it would might seem at a first glance. The better theory−experiment agreement for **VIII** and **X** might be, to a certain extent, due to the larger blueshift of the absorption bands (2850 and 3178 cm^{-1}, respectively) compared to **I** (only 481 cm^{-1}) for (SS,neq), combined with a large Stokes shift for all three systems (see the following section). Therefore, if the absorption maximum is accurate, the emission is strongly redshifted. On the other hand, when the absorption maximum is strongly blueshifted then the prediction of the emission maximum is reasonably accurate. The reason for the large Stokes shift might be the overestimation of geometrical displacements upon ES relaxation, but a definite answer to this issue is given in the Vibronic Spectra section. Turning now to the performance of the various solvation methods, one notices that the LR model in its equilibrium limit leads to larger

Table 5. Theoretical Estimates of Stokes Shifts and 0−0 Energies Using Different Solvation Models along with Their Experimental Counterparts[a]

system	ΔE^{Stokes} (LR,eq)	ΔE^{Stokes}(SS,eq)	ΔE^{Stokes}(SS,neq)	$\Delta E^{\text{Stokes}}_{\text{Exp.}}$	E^{AFCP}(SS,neq)	$E^{0-0}_{\text{Exp.}}$
I	8219	8146	8283	1990 (2149)	15 357	18 124
II	7840	7775	7775		16 220	
III	9219	8566	8662		15 566	
IV	8162	7783	8074		18 623	
V	7670	7630	7630		12 631	
VI	7678	7501	7759		16 075	
VII	7848	7670	7880		16 373	
VIII	7154	6936	6944	3099 (4210)	21 446	20 367
IX	7428	7259	7404		16 405	
X	7114	6952	6952	3377 (4174)	17 422	15 907
XI	5275	5033	5025		15 599	
XII	9340	9227	9227		16 236	
XIII	8195	7920	8041		17 551	
XIV	8743	8275	8525		17 502	
MSE	4674	4523	4571		−58	
MAE	4674	4523	4571		1787	

[a]All quantities are given in cm^{-1}. Values obtained from lineshape spectra are given in parentheses. At the bottom of the Table MSE and MAE are given as well, see caption to Table 4 for more details.

errors than SS. The results are practically unaltered between fully equilibrium and nonequilibrium SS solvation for all three molecules since nonpolar solvents are used. For the rest of the molecules for which no experimental data exist both the (SS,eq) and (SS,neq) give similar results while, on the other hand, there are more pronounced differences between SS and LR solvation. A last point of importance is the use of the experimental lineshapes to extract the absorption (emission) maxima. Whereas for the case of the absorption using either the spectra themselves or the lineshapes gives the same maxima, for the case of emission they can differ substantially as can be seen from the values in parentheses in Table 4. Based on the lineshapes, the error panels for emission are, in general, slightly reduced for **VIII** and **X** (0.63−3.24%, depending on the solvation model used) but do not improve the very poor theory-experiment agreement found for **I**.

In brief, although for emission the available experimental data are not sufficient so as to draw significant conclusions on the adequacy of the vertical approximation in reproducing experimental the positions of emission maxima, for the case of absorption the approach is sufficiently accurate in both LR and SS formalisms. Further insights on appropriateness of the vertical approach will be given in the next sections, in which the vibronic absorption and emission bands of **I**, **VIII**, and **X** are discussed.

4.2. 0−0 Energies and Stokes Shifts. Let us now turn towards the reproduction of the experimentally observed Stokes shifts and 0−0 energies, the latter being taken as the point of intersection of the absorption and emission bands (absorption−fluorescence crossing point, AFCP).[62,92] The results are gathered in Table 5. Looking at the theory-experiment comparisons for molecules **I**, **VIII**, and **X**, it becomes obvious that theory severely overestimates the experimental Stokes shifts, irrespectively of the solvation model used. The relative error reaches up to almost 300% of the experimental value for the case of **I** while for the other two systems the errors are lower but still unsatisfactory. Using the experimental lineshapes to compute the Stokes shift improves the agreement between theory and experiment for all the three systems irrespectively of the solvation model used, especially for **VIII** and **X**, for which, the error reduction reaches up to half the original value. It seems that while the vertical transition approximation permits a reasonable estimation of absorption band maxima themselves, it leads to excessive errors when computing the Stokes shifts. This can be explained by considering that when transition maxima are computed, it is the magnitude of the shifts with respect to experimental maxima that are evaluated and not their sign (blueshift or redshift). On the other hand, the calculation of Stokes shifts is much more sensitive to the errors introduced especially in the geometries.

Focusing now on the theoretical estimates for the 0−0 energies, we notice that they agree quite well with the experimental estimates. A rather large theory-experiment discrepancy is seen for molecule **I** with theory underestimating the experimental value by roughly 15%. For the other two molecules, namely **VIII** and **X**, theory overshoots the measured value but the relative errors remain quite small. In fact, for the cases where the absorption maximum is strongly overestimated (**VIII** and **X**) (SS,neq) there is a small error on the AFCP (1079 and 1515 cm^{-1}, respectively). On the contrary, for system **I** for which the absorption maximum is accurate, the error on the AFCP is large. In overall, it seems that the currently employed theoretical model is able to provide quite reliable estimates for the 0−0 energies for each particular system, although it cannot reproduce the experimental relative ordering for the three diarylethenes mentioned above. Nonetheless, it has to be emphasized that three molecules constitute a too small set making it difficult to reach general conclusions.

In light of the aforementioned errors, especially for the Stokes shifts, and in order to investigate all the possible sources of error, we have considered the possibility of emission from the S_2 state instead from the S_1. Therefore, we have computed the 0−0 energies and Stokes shifts based on the $S_0 \rightarrow S_1$ and $S_2 \rightarrow S_0$ transition energies. The results for the three molecules exhibiting emission are gathered in Tables S−IV and S−V (see the SI) from which it can be seen that, for the case of S_2 emission, the errors for the 0−0 energies are much larger (27.5−58.0%) than the ones deduced based on the emission from the S_1 (5.3−15.3%). A conclusive answer to the question

dx.doi.org/10.1021/ct500371u | J. Chem. Theory Comput. 2014, 10, 3944−3957

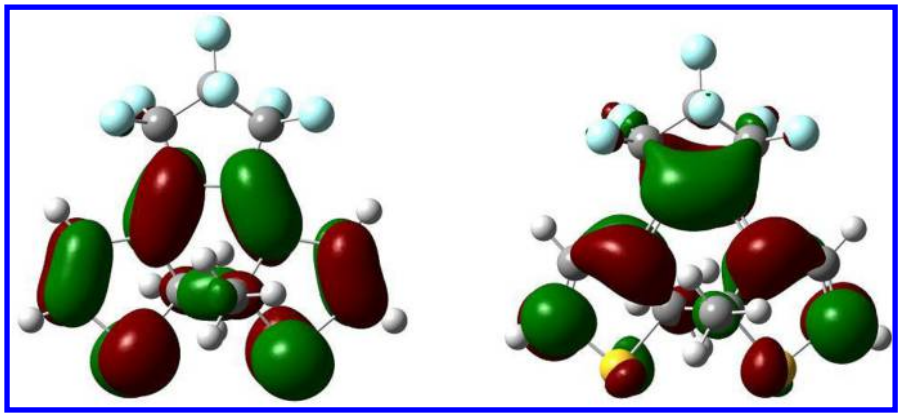

Figure 4. Occupied (left) and virtual (right) NTO corresponding to the $S_0 \rightarrow S_1$ transition of the prototypical diarylethene at its GS geometry. The selected contour threshold corresponds to 0.03 au.

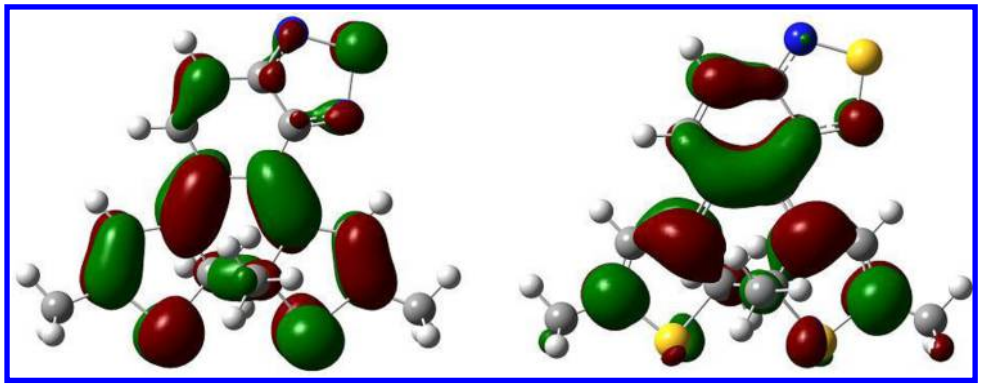

Figure 5. Occupied (left) and virtual (right) NTO corresponding to the $S_0 \rightarrow S_1$ transition of **II** at its GS geometry. The selected contour threshold corresponds to 0.03 au.

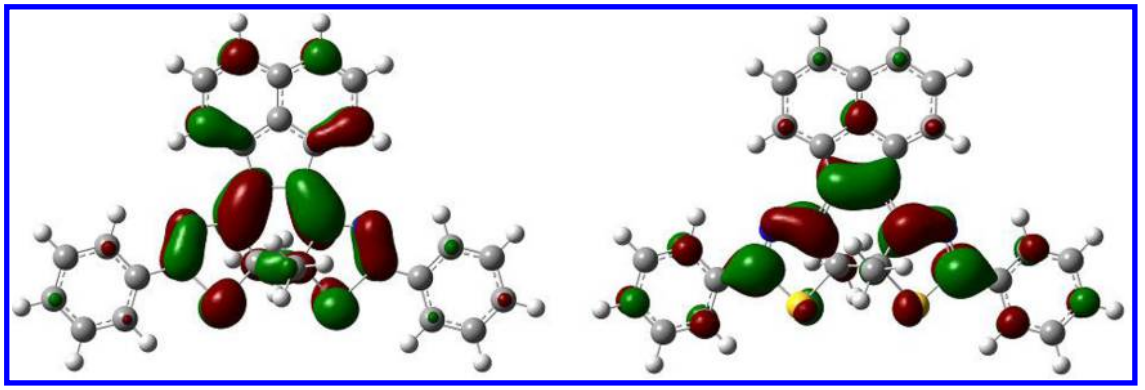

Figure 6. Occupied (left) and virtual (right) NTO corresponding to the $S_0 \rightarrow S_1$ transition of **X** at its GS geometry. The selected contour threshold corresponds to 0.03 au.

of a possible S_2 fluorescence is given from the Stokes shifts which, for the case of emission from the second excited state, are negative for all systems considered; a finding that is not compatible with the experimental findings. It can be therefore safely concluded that the experimental emission spectra are due to the $S_1 \rightarrow S_0$ and that the previously discussed theory-experiment discrepancies cannot be explained by the violation of Kasha's rule.

4.3. Correlation Between Geometrical and Optical Properties. In order to aid the rational design of diarylethenes having specific properties it is of interest to relate structural properties such as the BLA_{scaled} in the GS with the optical properties of the studied molecules, such as the maximum absorption wavelength λ_{max}. In fact a correlation has been found between the two aforementioned quantities in a previous article focusing mainly on thiophene-substituted diarylethenes.[88] As can be shown in Figure S-5 in Supporting Information, for the case of experiment, there is no correlation between BLA and absorption λ_{max}. The same picture emerges for all theoretical models employed, for which the determination coefficients R^2 are lower than 0.1. As an example, the BLA_{scaled} and λ_{max} of each molecule for the case of (SS,neq) solvation are also available in Figure S-5 in Supporting Information. The reason for the absence of structural−optical property correlation is obviously the significant structural diversity of the investigated diarylethenes. Despite the fact that for all systems the $S_0 \rightarrow S_1$

transition involves predominantly excitation from the HOMO to the LUMO, the orbitals might exhibit different topologies as can be seen in Figures 4−6 for the case of the prototypical diarylethene, **II**, and **X**, respectively. For the prototypical diarylethene, the redistribution of charge takes place on the cyclohexadiene core and the thiophene rings. On the other hand, the redistribution of charge in **II** and **X** involves also the conjugated bridges. For **II**, the significant charge transfer toward the bridge is due to the electron withdrawing character of the dithiazole group, in contrast to what is seen for **X** where the bridge acts similar to a donor. The lack of the aforementioned correlations can be considered as a warning: structure-properties relationships are only meaningful for subsets composed of structurally similar photochromes.

4.4. Functional and Basis Set Effects. To investigate the influence of the basis set employed, we have also used the large 6-311+G(2d,p) atomic basis set in conjunction with the ωB97X-D functional for all systems while the influence of the chosen functional on the quality of the obtained results has been examined by employing the ωB97 and ωB97X ones along with the 6-31G(d) atomic basis set for **I**, **VIII**, and **X**. The results for the two latter functionals used can be found in Table S-II in Supporting Information. The vertical excitation energies (in cm^{-1}) tend to increase by passing from the ωB97X-D to ωB97, that is, the follow the order ωB97 > ωB97X > ωB97X-D, which holds for all methods (SS and LR) using equilibrium and nonequilibrium solvation. This is the expected trend in the members of the ωB97 family of functionals for the case of absorption energies.[91] More interestingly, the aforementioned ordering holds also for the emission energies (SS, LR, equilibrium, and nonequilibrium) of the three systems. The average deviations of ωB97 and ωB97X with respect to the ωB97X-D results are quite large for the case of absorption, reaching up to 2767 and 1818 cm^{-1}, respectively, while for the emission energies they are smaller. Nonetheless, the examined functionals seem to have a systematic and predictable performance for the systems under study, and they tend to yield larger average deviations with respect to experiment, therefore validating the use of ωB97X-D as the functional of choice in this work. Of course, better results could be obtained by using optimally tuned ω values[93−97] but at the cost of numerous additional calculations. In that framework, it is worth to pinpoint the work of Okuno et al. who tuned the CAM-B3LYP range-separated hybrid to reach a better description of the absorption wavelengths of several diarylethenes.[56,98]

The influence of the atomic basis set employed in the calculation is less pronounced than that of the functional used, as can be seen from the contents of Table S-III in Supporting Information. Using the large 6-311+G(2d,p) basis set leads to a decrease of the vertical (LR,neq) absorption energies (in cm^{-1}) compared to the 6-31G(d) results for all diarylethenes, the mean absolute difference being very small: 581 cm^{-1}. Therefore, our selected 6-31G(d) basis set provides a very good compromise between accuracy and computational cost, at least for the vertical absorption energies.

5. VIBRONIC SPECTRA

Absorption and emission experimental spectra are available for **I**, **VIII**, and **X**, and we have carried out their simulation at 298 K. As discussed in the previous sections, for large molecules undergoing significant structural displacement during the spectroscopic transition, the AH model formulated in Cartesian coordinates may fail due to the inadequacy of such coordinate frame to properly account for the curvilinear displacement connecting the initial and final state minimum structures. In such cases, the use of either internal coordinates or the VH model in Cartesian coordinates have shown to lift, at least partially, such limitations.[99,100] In the case of diarylethenes, the AH model actually fails to provide plausible simulated spectra, while the VH delivers reasonable results (see Figure S-8 in the SI). A close inspection to both the Duschinsky matrix and the displacement vector (see Figures S-6 and S-7 in the SI) reveals that the main source of error in the AH model, arises from spurious couplings in the Duschinsky matrix, in agreement with previous results for carotenoids.[100] The simulated spectra with the VH model for the three molecules are presented in Figure 7.

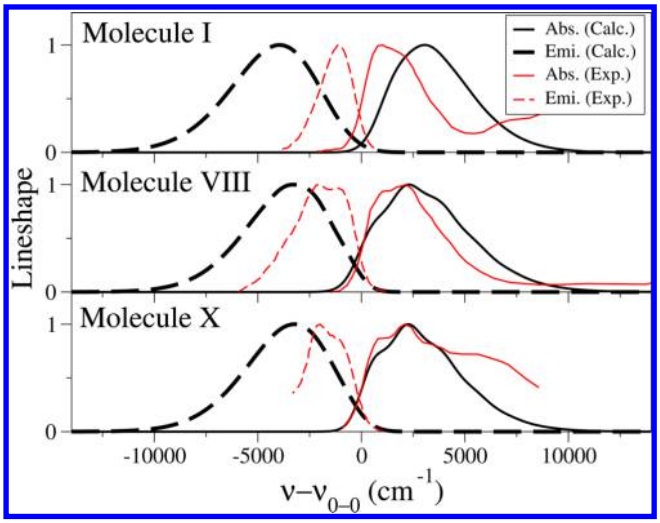

Figure 7. Absorption and emission spectrum simulated at 298 K for molecules **I**, **VIII**, and **X** with the VH model. A broadening function is added to all the spectra with HWHM = 242 cm^{-1} (0.03 eV). The experimental spectra are extracted from the literature works[23,63,67] and included for comparison. The frequency values are reported relative to the 0−0 energies given in Table 5.

The computed absorption for species **X** nicely reproduces the main vibronic progression, assigned to a C−C stretching (see below), although the intensity of the lowest-energy peak is underestimated. A similar situation seems to hold for molecule **VIII** where however the two lowest-energy peaks almost collapse in a single broad band in the experiment. From Figure 7, it is evident that the error of the Stokes shift is more relevant for molecule **I**, as already concluded from the data in Table 5. Interestingly, the Stokes shifts computed from the simulated spectra improve the estimates obtained directly from the vertical energies shown in Table 5; concretely the shifts from the simulations are 7002, 5603, and 5503 cm^{-1} for molecules **I**, **VIII**, and **X**, respectively. For the latter two molecules, these values are overestimated by only ∼1400 cm^{-1} with respect to experiment, while the error is still remarkable for molecule **I**. It should be highlighted, however, that the estimates given in Table 5 provide the right qualitative trend at a lower computational cost. Furthermore, despite being superior to the AH model for the three investigated systems, VH results still remarkably overestimate the bandwidth of both the absorption and, more significantly, the emission spectra as compared to the experimental ones.[101] A correlated aspect is the steepness of absorption and emission close to their

intersection: computations nicely reproduce it for the absorption of **VIII** and **X** while underestimate the slope of the emission; for molecule **I**, the rise of both absorption and (even more) emission is predicted to be too slow. It is noteworthy that such larger errors in the broadening of the emission spectra have been already encountered in other systems.[87] In order to analyze this finding, we focus on the emission spectrum of molecule **X**, since the conclusions for this system apply also to the rest of them. Large displacements are observed in both low frequency (bending of the molecular plane) and high frequency (C−C stretching along the π-conjugated system) modes. Such mode displacements lead to vibrational progressions that have a deep impact on the spectrum shape, giving rise to a band much broader than in the experiment and without a clear vibrational structure. Concretely, low-frequency progressions cause a marked temperature dependence of the spectral shape and wash out the vibrational signatures at room temperature. On the other hand, progressions arising from high-frequency modes lead to a large width independently of the temperature. In order to clearly illustrate both effects, we exploited the block-diagonal form of the Duschinsky matrix and deconvoluted the total spectrum into those corresponding to each block of modes: one involving the C−C stretching modes and the one with the remaining modes.

The spectra are shown in Figure 8. It is observed that the block with the largely displaced C−C stretching modes is the main responsible for the width of the spectrum, while the low-frequency modes cause the blurring of the vibronic shape of the spectrum, contributing to the spectral width to a lower extent. The latter effect is strongly dependent on temperature, as shown in the Supporting Information (see Figure S-9) and might be partially biased by the fact that harmonic approximation is not well suited to describe modes with very low frequency. The identification of the C−C stretching progressions as the main responsible for the spectral width is further confirmed by a time-independent simulation of the spectrum at 0 K. It is worth noticing that simulations with the Vertical Gradient (VG) model, in which the Duschinsky matrix is set to the identity matrix, provide a spectrum similar to that obtained with the VH model (see Figure S-10 of the Supporting Information), indicating that the vibronic progressions are mainly due to normal mode displacements. Therefore, our results suggest that ωB97X-D calculations overestimate the displacements along these modes. A further confirmation is given by the underestimation of the intensity of the lowest-energy peak in the absorption of **VIII** and **X**. To explore this further, we have performed computations on a test model system (see Figure S-11 in Supporting Information). Since CASSCF geometries for both the S_0 and the S_1 are readily available[33] for this system, it is worthwhile to see how (TD-)DFT performs compared to an *ab initio* method. The most important geometrical parameters for the CAS(10,10)/6-31G(d) and (TD-)DFT ωB97X-D/6-31G(d) optimized geometries are shown in Figure S-11 in Supporting Information while their differences in the bond distances are summarized in Figures S-12 and S-13 in Supporting Information for the GS and ES geometries, respectively. The results suggest that there is no systematic tendency of TD-DFT in overestimating the geometrical changes by passing from the GS to the ES optimized geometries compared to CASSCF. Nonetheless, it has to be noted that CASSCF is not the golden standard in *ab initio* methods due to the lack of dynamic correlation, and therefore, a verdict can be reached only after comparing TD-DFT ES geometries with the corresponding CASPT2 and EOM-CCSD ones. At the moment this is unfeasible due to the size of the systems and therefore our proposed explanation for the large Stokes shifts and broadening of the spectra still needs to be investigated further. Moreover, other sources of spurious mode displacement, such as the limitations of Cartesian coordinates to describe large normal mode amplitudes, should be considered.

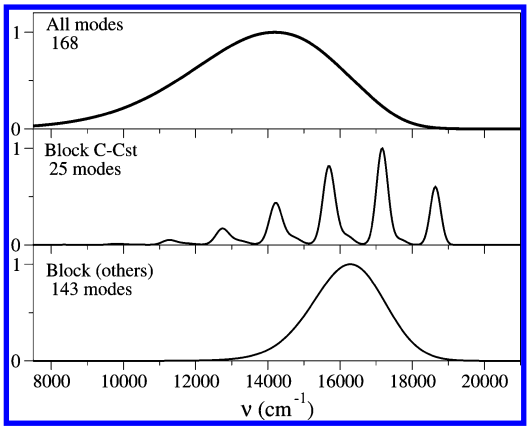

Figure 8. Emission spectrum simulated at 298 K for molecule **X** with the VH model. The total spectrum (top panel) can be deconvoluted in the spectra arising from C−C stretching modes (medium panel) and from the remaining modes (lower panel). A broadening function is added to all the spectra with HWHM = 242 cm^{-1} (0.03 eV) for the total spectrum and HWHM = $(242/\sqrt{2})$ cm^{-1} for each block.

As a last point of importance, we have also investigated the errors that arise from the harmonic treatment used to compute the vibronic spectra. One approach to partially fix the issues of such an approximation is to use the anharmonic fundamental frequencies but keeping the harmonic representation to evaluate the FC integrals. The separation between vibronic emission features along the progression due to the C−C stretching modes is reduced when GS anharmonic frequencies are used (see Figure S-14 in Supporting Information), thus partially reducing the overall width. However, such differences cannot account for all the overbroadening observed in the simulated spectra, suggesting that the overestimation of the normal mode displacement is still relevant.

6. CONCLUSIONS

An analysis of the structure and optical properties of a large number of diarylethenes in their closed form has been performed employing TD-DFT at the ωB97X-D/6-31G(d) level and using the PCM model to describe the bulk solvent effects. The present study is the first to address the relaxation of nontrivial DTEs after the initial photoexcitation and has permitted us to calculate, in a concise manner, the vertical absorption and emission energies, 0−0 energies and the Stokes shifts. The analysis of the DTE structures has revealed that there are significant geometrical rearrangements on the cyclohexadiene core both due to substitution (GS) and relaxation after photoexcitation (ES). As far as the optical properties are concerned, the abundance of experimental data for the case of absorption has permitted us to extensively investigate the performance of our theoretical models. The vertical approximation was found to be adequate for a fair

agreement between theory and experiment in most of the cases, with TD-ωB97X-D tending to overestimate the experimental values. Moreover, a comparison of the different solvation models has shown that both the equilibrium and non-equilibrium solvation limits give practically identical results for absorption, even when polar solvents are used. This behavior was attributed to a spatially localized electronic redistribution upon photoexcitation, which does not strongly influence the polarity of the molecules. For emission, the limited number of experimental data made it impossible to reach general conclusions, although the selected model seems to perform quite well for the studied cases. Moreover, while the calculated 0−0 energies are in good agreement with their experimental counterparts, this does not hold for the case of Stokes shifts for which large discrepancies were found when the ωB97X-D functional is used. Finally, the simulation of the vibronic spectra using a vertical model (VH) allows to significantly improve the estimate of the Stokes shifts pointing out the relevance of vibronic effects, and to correctly reproduce the main vibronic progression of the absorption of **VIII** and **X**. Moreover, it permits to individuate the geometric displacements of the π-conjugated system that are mainly responsible for the vibrational structure and the width of the spectra. Actually, our simulations produce an excessive broadening compared to experiment, suggesting a possible overestimation of the geometrical displacements, between the initial and final electronic states, computed at the TD-DFT level. The errors on the S_0/S_1 displacements, which are connected to the prediction of a too large broadening, also lead to an overestimation of the gaps between the 0−0 and maximum frequencies of absorption and emission (Δ_{abs} and Δ_{emi}, respectively) and ultimately of the Stokes shift ($|\Delta_{abs}| + |\Delta_{emi}|$). On these grounds, the errors on the Stokes shift can be at least partially traced back to the inaccuracies of the aforementioned S_0/S_1 displacements. We should note, however, that despite this structural inaccuracy, the quality of the predicted optical data supports the use of TD-DFT to investigate the spectroscopic properties of these compounds.

In conclusion, it has to be emphasized once more that the performance of TD-DFT in reproducing emission properties for diarylethenes remains hard to establish due to the lack of available experimental data, and it is our hope that this will change in the coming years by a more systematic interplay between theory and experiment.

■ ASSOCIATED CONTENT

Supporting Information

Additional NTO plots. Comparisons of GS and ES optimized geometries in the gas and liquid phases. Functional and atomic basis set benchmarks. Correlation diagrams between experimental and theoretical absorption maxima for different solvation models. Optical properties based on the emission from the S_2 state. Structure−absorption maximum correlation diagram. Representation of the Duschinsky matrix and normal mode displacements with the AH and VH models for molecule **X**. Simulated emission spectra of molecule **X** with the AH and VH models, including separated blocks of modes. Emission spectra for molecule **X** simulated with the VH model at different temperatures. Absorption and emission spectra for molecule **X** using both the VH and VG models. (TD-)DFT and CASSCF optimized structures at the GS and ES for the model system. Comparisons between (TD-)DFT and CASSCF bond lengths of the model system at the GS and ES optimized geometries. Harmonic and anharmonic vibrationally resolved emission spectra for the model system using the VH model. This material is available free of charge via the Internet at http://pubs.acs.org/.

■ AUTHOR INFORMATION

Corresponding Authors

*Email: fabrizio.santoro@iccom.cnr.it.

*Email: Denis.Jacquemin@univ-nantes.fr.

Notes

The authors declare no competing financial interest.

■ ACKNOWLEDGMENTS

A.C. thanks the European Research Council (ERC, Marches-278845) for his postdoctoral grant. D.J. acknowledges the European Research Council (ERC) and the *Région des Pays de la Loire* for financial support in the framework of a Starting Grant (Marches 278845) and a *recrutement sur poste stratégique*, respectively. This research used resources of (1) CCIPL (*Centre de Calcul Intensif des Pays de Loire*) and (2) a local Troy cluster. This work was partially supported by the Italian MIUR (PRIN 2010-2011 2010ERFKXL).

■ REFERENCES

(1) Tamai, N.; Miyasaka, H. *Chem. Rev.* **2000**, *100*, 1875−1890.

(2) Szaciłowski, K. *Chem. Rev.* **2008**, *108*, 3481−3548.

(3) Kawata, S.; Kawata, Y. *Chem. Rev.* **2000**, *100*, 1777−1788.

(4) Dürr, H.; Bouas-Laurent, H. *Photochromism: Molecules and Systems*; Elsevier: New York, 2003; pp 1−1218.

(5) Zhang, J.; Wang, J.; Tian, H. *Mater. Hor.* **2014**, *1*, 69−184.

(6) Nakamura, S.; Yokojima, S.; Uchida, K.; Tsujioka, T. *J. Photochem. Photobiol., C* **2011**, *12*, 138−150.

(7) Yokoyama, Y.; Kose, M. *J. Photochem. Photobiol., A* **2004**, *166*, 9−18.

(8) Nakamura, A.; Yokojima, S.; Uchida, K.; Tsujioka, T.; Goldberg, A.; Murakami, A.; Shinoda, K.; Mikami, M.; Kobayashi, T.; Kobatake, S.; Matsuda, K.; Irie, M. *J. Photochem. Photobiol., A* **2008**, *200*, 10−18.

(9) Matsuda, K.; Irie, M. *J. Photochem. Photobiol., C* **2004**, *5*, 169−182.

(10) Yun, C.; You, J.; Kim, J.; Kim, E. *J. Photochem. Photobiol., C* **2009**, *10*, 111−129.

(11) Fukaminato, T. *J. Photochem. Photobiol., C* **2011**, *12*, 177−208.

(12) Tian, H.; Yang, S. *Chem. Soc. Rev.* **2004**, *33*, 85−97.

(13) Irie, M. *Chem. Rev.* **2000**, *100*, 1685−1716.

(14) Irie, M. *Photochem. Photobiol. Sci.* **2010**, *9*, 1535−1542.

(15) *New Frontiers in Photochromism*; Irie, M., Yokoyama, Y., Seki, T., Eds.; Springer: New York, 2013; pp 1−298.

(16) Perrier, A.; Maurel, F.; Jacquemin, D. *Acc. Chem. Res.* **2012**, *45*, 1173−1182.

(17) Irie, M.; Mohri, M. *J. Org. Chem.* **1988**, *53*, 803−808.

(18) Nakayama, Y.; Hayashi, K.; Irie, M. *J. Org. Chem.* **1990**, *55*, 2592−2596.

(19) Irie, M.; Sayo, K. *J. Phys. Chem.* **1992**, *96*, 7671−7674.

(20) Gilat, S. L.; Kawai, S. H.; Lehn, J. M. *J. Chem. Soc., Chem. Commun.* **1993**, 1439−1442.

(21) Woodward, R. B.; Hoffman, R. *The Conservation of Orbital Symmetry*; Verlag Chemie: Weinheim, 1970; pp 1−177.

(22) Fukagawa, M.; Kawamura, I.; Ubukata, T.; Yokoyama, Y. *Chem.—Eur. J.* **2013**, *19*, 9434−9437.

(23) Pang, S.-C.; Hyun, H.; Lee, S.; Jang, D.; Lee, M. J.; Kang, S. H.; Ahn, K. H. *Chem. Commun.* **2012**, *48*, 3745−3747.

(24) Szymański, W.; Beierle, J.; Kistemaker, H.; Velema, W.; Feringa, B. L. *Chem. Rev.* **2013**, *113*, 6114−6178.

(25) Zou, Y.; Yi, T.; Xiao, S.; Li, F.; Li, C.; Gao, X.; Wu, J.; Yu, M.; Huang, C. *J. Am. Chem. Soc.* **2008**, *130*, 15750−15751.

(26) Matsuda, K. *Pure Appl. Chem.* **2008**, *80*, 555−561.

(27) Lim, S.-J.; Seo, J.; Park, S. Y. *J. Am. Chem. Soc.* **2006**, *128*, 14542−14547.
(28) Raymo, F. M.; Tomasulo, M. *Chem. Soc. Rev.* **2005**, *34*, 327−336.
(29) Fukaminato, T.; Doi, T.; Tamaoki, N.; Okuno, K.; Ishibashi, Y.; Miyasaka, H.; Irie, M. *J. Am. Chem. Soc.* **2011**, *133*, 4984−4990.
(30) Boggio-Pasqua, M.; Ravaglia, M.; Bearpark, M. J.; Garavelli, M.; Robb, M. A. *J. Phys. Chem. A* **2003**, *107*, 11139−11152.
(31) Patel, P. D.; Masunov, A. E. *J. Phys. Chem. C* **2011**, *115*, 10292−10297.
(32) Mikhailov, I. A.; Belfield, K. D.; Masunov, A. E. *J. Phys. Chem. A* **2009**, *113*, 7080−7089.
(33) Perrier, A.; Aloise, S.; Olivucci, M.; Jacquemin, D. *J. Phys. Chem. Lett.* **2013**, *4*, 2190−2196.
(34) Staykov, A.; Areephong, J.; Browne, W. R.; Feringa, B. L.; Yoshizawa, K. *ACS Nano* **2011**, *5*, 1165−1178.
(35) Nakamura, S.; Kobayashi, T.; Takata, A.; Uchida, K.; Asano, Y.; Murakami, A.; Goldberg, A.; Guillaumont, D.; Yokojima, S.; Kobatake, S.; Irie, M. *J. Phys. Org. Chem.* **2007**, *20*, 821−829.
(36) Patel, P. D.; Mikhailov, I. A.; Belfield, K. D.; Masunov, A. E. *Int. J. Quantum Chem.* **2009**, *109*, 3711−3722.
(37) Guillaumont, D.; Kobayashi, T.; Kanda, K.; Miyasaka, H.; Uchida, K.; Kobatake, S.; Shibata, K.; Nakamura, S.; Irie, M. *J. Phys. Chem. A* **2002**, *106*, 7222−7227.
(38) Asano, Y.; Murakami, A.; Kobayashi, T.; Goldberg, A.; Guillaumont, D.; Yabushita, S.; Irie, M.; Nakamura, S. *J. Am. Chem. Soc.* **2004**, *126*, 12112−12120.
(39) Uchida, K.; Guillaumont, D.; Tsuchida, E.; Mochizuki, G.; Irie, M.; Murakami, A.; Nakamura, S. *J. Mol. Struct. (THEOCHEM)* **2002**, *579*, 115−120.
(40) Aloise, S.; Sliwa, M.; Buntinx, G.; Delbaere, S.; Perrier, A.; Maurel, F.; Jacquemin, D.; Takeshita, M. *Phys. Chem. Chem. Phys.* **2013**, *15*, 6226−6234.
(41) Wiebeler, C.; Bader, C.; Meier, C.; Schumacher, S. *Phys. Chem. Chem. Phys.* **2014**, DOI: 10.1039/c3cp55490b.
(42) Perrier, A.; Maurel, F.; Browne, W. R.; Jacquemin, D. *Chem. Commun.* **2013**, *49*, 4247−4249.
(43) Jacquemin, D.; Perpète, E. A.; Maurel, F.; Perrier, A. *J. Phys. Chem. C* **2010**, *114*, 9489−9497.
(44) Perrier, A.; Maurel, F.; Jacquemin, D. *J. Phys. Chem. C* **2011**, *115*, 9193−9203.
(45) Cipolloni, M.; Heyndericckx, A.; Maurel, F.; Perrier, A.; Jacquemin, D.; Siri, O.; Ortica, F.; Favaro, G. *J. Phys. Chem. C* **2011**, *115*, 23096−23106.
(46) Jacquemin, D.; Perpète, E. A.; Maurel, F.; Perrier, A. *J. Phys. Chem. Lett.* **2010**, *1*, 2104−2108.
(47) Jacquemin, D.; Perpète, E. A.; Maurel, F.; Perrier, A. *J. Phys. Chem. Lett.* **2010**, *1*, 434−438.
(48) Jacquemin, D.; Michaux, C.; Perpète, E. A.; Maurel, F.; Perrier, A. *Chem. Phys. Lett.* **2010**, *488*, 193−197.
(49) Perrier, A.; Tesson, S.; Jacquemin, D.; Maurel, F. *Comput. Theor. Chem.* **2012**, *990*, 167−176.
(50) Ashraf, M.; Bruque, N.; Tan, J.; Beran, G.; Lake, R. *J. Chem. Phys.* **2011**, *134*, 024524.
(51) Jacquemin, D.; Perpète, E. A. *Chem. Phys. Lett.* **2006**, *429*, 147−152.
(52) Chen, D.; Wang, Z.; Zhang, H. *J. Mol. Struct. (THEOCHEM)* **2008**, *859*, 11−17.
(53) Perpète, E. A.; Jacquemin, D. *J. Photochem. Photobiol. A: Chem.* **2007**, *187*, 40−44.
(54) Laurent, A. D.; André, J. M.; Perpète, E. A.; Jacquemin, D. *J. Photochem. Photobiol. A: Chem.* **2007**, *192*, 211−219.
(55) Maurel, F.; Perrier, A.; Perpète, E. A.; Jacquemin, D. *J. Photochem. Photobiol. A: Chem.* **2008**, *199*, 211−223.
(56) Okuno, K.; Shigeta, Y.; Kishi, R.; Miyasaka, H.; Nakano, M. *J. Photochem. Photobiol., A* **2012**, *235*, 29−34.
(57) Jacquemin, D.; Perpète, E. A.; Maurel, F.; Perrier, A. *Phys. Chem. Chem. Phys.* **2010**, *12*, 13144−13152.
(58) Perpète, E. A.; Maurel, F.; Jacquemin, D. *J. Phys. Chem. A* **2007**, *111*, 5528−5535.
(59) Clark, A. E. *J. Phys. Chem. A* **2006**, *110*, 3790−3796.
(60) Dierksen, M.; Grimme, S. *J. Phys. Chem. A* **2004**, *108*, 10225−10237.
(61) Send, R.; Kühn, M.; Furche, F. *J. Chem. Theory Comput.* **2011**, *7*, 2376−2386.
(62) Jacquemin, D.; Planchat, A.; Adamo, C.; Mennucci, B. *J. Chem. Theory Comput.* **2012**, *8*, 2359−2372.
(63) Takagi, Y.; Kunishi, T.; Katayama, T.; Ishibashi, Y.; Miyasaka, H.; Morimoto, M.; Irie, M. *Photochem. Photobiol. Sci.* **2012**, *11*, 1661−1665.
(64) Zhu, W.; Meng, X.; Yang, Y.; Zhang, Q.; Xie, Y.; Tian, H. *Chem.—Eur. J.* **2010**, *16*, 899−906.
(65) Li, Z.; Xia, J.; Liang, J.; Yuan, J.; Jin, G.; Yin, J.; Yu, G.-A.; Liu, S. *Dyes Pigm.* **2011**, *90*, 290−296.
(66) Xie, N.; Chen, Y. *J. Mater. Chem.* **2007**, *17*, 861−865.
(67) Fukumoto, S.; Nakagawa, T.; Kawai, S.; Nakashima, T.; Kawai, T. *Dyes Pigm.* **2011**, *89*, 297−304.
(68) Jeong, Y. C.; Yang, S. I.; Ahn, K. H.; Kim, E. *Chem. Commun.* **2005**, 2503−2505.
(69) Meng, X.; Zhu, W.; Zhang, Q.; Feng, Y.; Tan, W.; Tian, H. *J. Phys. Chem. B* **2008**, *112*, 15636−15645.
(70) Kitai, J.-I.; Kobayash, T.; Uchida, W.; Hatakeyama, M.; Yokojima, S.; Nakamura, S.; Uchida, K. *J. Org. Chem.* **2012**, *77*, 3270−3276.
(71) Suzuki, K.; Ubukata, T.; Yokoyama, Y. *Chem. Commun.* **2012**, *48*, 765−767.
(72) Liu, H.-H.; Chen, Y. *J. Phys. Chem. A* **2009**, *113*, 5550−5553.
(73) Kose, M.; Orhan, E.; Suzuki, K.; Tutar, A.; Ünlü, C.; Yokoyama, Y. *J. Photochem. Photobiol., A* **2013**, *257*, 50−53.
(74) Giraud, M.; Léaustic, A.; Charlot, M. F.; Yu, P.; Césario, M.; Philouze, C.; Pansu, R.; Nakatani, K.; Ishow, E. *New. J. Chem.* **2005**, *29*, 439−446.
(75) Chai, J. D.; Head-Gordon, M. *Phys. Chem. Chem. Phys.* **2008**, *10*, 6615−6620.
(76) Frisch, M. J.; Trucks, G. W.; Schlegel, H. B.; Scuseria, G. E.; Robb, M. A.; Cheeseman, J. R.; Scalmani, G.; Barone, V.; Mennucci, B.; Petersson, G. A.; Nakatsuji, H.; Caricato, M.; Li, X.; Hratchian, H. P.; Izmaylov, A. F.; Bloino, J.; Zheng, G.; Sonnenberg, J. L.; Hada, M.; Ehara, M.; Toyota, K.; Fukuda, R.; Hasegawa, J.; Ishida, M.; Nakajima, T.; Honda, Y.; Kitao, O.; Nakai, H.; Vreven, T.; Montgomery, J. A., Jr.; Peralta, J. E.; Ogliaro, F.; Bearpark, M.; Heyd, J. J.; Brothers, E.; Kudin, K. N.; Staroverov, V. N.; Kobayashi, R.; Normand, J.; Raghavachari, K.; Rendell, A.; Burant, J. C.; Iyengar, S. S.; Tomasi, J.; Cossi, M.; Rega, N.; Millam, J. M.; Klene, M.; Knox, J. E.; Cross, J. B.; Bakken, V.; Adamo, C.; Jaramillo, J.; Gomperts, R.; Stratmann, R. E.; Yazyev, O.; Austin, A. J.; Cammi, R.; Pomelli, C.; Ochterski, J. W.; Martin, R. L.; Morokuma, K.; Zakrzewski, V. G.; Voth, G. A.; Salvador, P.; Dannenberg, J. J.; Dapprich, S.; Daniels, A. D.; Farkas, O.; Foresman, J. B.; Ortiz, J. V.; Cioslowski, J.; Fox, D. J. *Gaussian 09 Revision C.01*; Gaussian, Inc.: Wallingford, CT, 2009.
(77) Chai, J. D.; Head-Gordon, M. *J. Chem. Phys.* **2008**, *128*, 084106.
(78) Li, X.; Frisch, M. J. *J. Chem. Theory Comput.* **2006**, *2*, 835−839.
(79) Barone, V. *J. Chem. Phys.* **2005**, *122*, 014108.
(80) Tomasi, J.; Mennucci, B.; Cammi, R. *Chem. Rev.* **2005**, *105*, 2999−3094.
(81) Improta, R.; Barone, V.; Scalmani, G.; Frisch, M. J. *J. Chem. Phys.* **2006**, *125*, 054103.
(82) Improta, R.; Scalmani, G.; Frisch, M. J.; Barone, V. *J. Chem. Phys.* **2007**, *127*, 074504.
(83) Avila Ferrer, F. J.; Santoro, F. *Phys. Chem. Chem. Phys.* **2012**, *14*, 13549−13563.
(84) (a) Santoro, F. *FCclasses*, a Fortran 77 code. http://village.pi.iccom.cnr.it (last accessed 20 Mar 2014), development version, 2013. (b) Cerezo, J.; Santoro, F. *TDspectrum, a routine for TD calculations within FCclasses*; 2013.
(85) Avila Ferrer, F.; Cerezo, J.; Soto, J.; Improta, R.; Santoro, F. *Comput. Theor. Chem.* **2014**, DOI: 10.1016/j.comptc.2014.03.003.

(86) Santoro, F.; Improta, R.; Lami, A.; Bloino, J.; Barone, V. *J. Chem. Phys.* **2007**, *126*, 084509.
(87) Avila Ferrer, F. J.; Cerezo, J.; Stendardo, E.; Improta, R.; Santoro, F. *J. Chem. Theory Comput.* **2013**, *9*, 2072−2082.
(88) Perrier, A.; Maurel, F.; Aubard, J. *J. Photochem. Photobiol. A: Chem.* **2007**, *189*, 167−176.
(89) Martin, R. L. *J. Chem. Phys.* **2003**, *118*, 4775−4777.
(90) Avila Ferrer, F. J.; Improta, R.; Santoro, F.; Barone, V. *Phys. Chem. Chem. Phys.* **2011**, *13*, 17007−17012.
(91) Jacquemin, D.; Perpète, E. A.; Ciofini, I.; Adamo, C. *Theor. Chem. Acc.* **2011**, *128*, 127−136.
(92) Goerigk, L.; Grimme, S. *J. Chem. Phys.* **2010**, *132*, 184103.
(93) Stein, T.; Kronik, L.; Baer, R. *J. Am. Chem. Soc.* **2009**, *131*, 2818−2820.
(94) Refaely-Ambrason, S.; Baer, R.; Kronik, L. *Phys. Rev. B* **2011**, *84*, 075144.
(95) Rudolph, M.; Autschbach, J. *J. Phys. Chem. A* **2011**, *115*, 14677−14686.
(96) Bernard, Y. A.; Shao, Y.; Krylov, A. I. *J. Chem. Phys.* **2012**, *136*, 204103.
(97) Jacquemin, D.; Moore, B.; Planchat, A.; Adamo, C.; Autschbach, J. *J. Chem. Theory Comput.* **2014**, *10*, 1677−1685.
(98) Okuno, K.; Shigeta, Y.; Kishi, R.; Nakano, M. *Chem. Phys. Lett.* **2013**, *585*, 201−206.
(99) Reimers, J. R. *J. Chem. Phys.* **2001**, *115*, 9103−9109.
(100) Cerezo, J.; Zuniga, J.; Requena, A.; Avila Ferrer, F. J.; Santoro, F. *J. Chem. Theory Comput.* **2013**, *9*, 4947−4958.
(101) It has to be noted here that for molecule **I** the experimental emission spectrum is much narrower than the absorption, remarkably violating mirror-symmetry. Having ruled out the possibility of emission from a state higher than the first one, this violation might suggest that the emitting species is not the same as the absorption species. A different isomer of **I** might be responsible for the emission since the upper part of the bridge of the molecule($S-CH_2-CH_2$) is rather floppy and may adopt a different conformation.